Suprathermal Electrons Generated by the Two-Plasmon-Decay Instability in Gas-Filled Hohlraums

Inertial confinement fusion (ICF) occurs when a spherical shell target containing thermonuclear fuel (i.e., deuterium and tritium) is imploded to produce energy gain.[1,2] Energy gain is predicted to be achieved with megajoule (MJ)-class lasers, such as the 192-beam, 351-nm, 1.8-MJ National Ignition Facility (NIF) being constructed at the Lawrence Livermore National Laboratory.[3] The implosion is driven by the ablation of material from the outer shell surface with intense laser beams (direct drive)[1] or with x rays produced in a high-Z enclosure or hohlraum (indirect drive).[2] Ignition will be first explored on the NIF with indirect-drive ICF. The NIF laser beams are arranged in two cones around the poles of the spherical target chamber to irradiate both sides of the cylindrical hohlraum through the laser entrance holes (LEH's). The laser beams irradiate the inner high-Z wall (i.e., Au, U) of the hohlraum, and the resulting high-Z plasma radiates x rays that are trapped and re-radiated by the opaque hohlraum wall and uniformly ablate the implosion capsule.[2,4] Ignition requires high-compression implosions (convergence ratio ~30), which places strict requirements on the irradiation-nonuniformity level of the x-ray drive on the capsule (<1% to 2% rms) and on the compressibility of the DT fuel. The required drive symmetry is more likely to be achieved if the hohlraum is filled with a low-Z gas fill, which minimizes the motion of the laser-deposition region.[2] A thin (0.5-μm) polyimide window covering each LEH is required to initially contain the gas fill. High compressibility requires that the DT fuel remain close to Fermi degenerate throughout the implosion. This requires control of irreversible heating of the DT fuel, leading to precise pulse shaping to minimize shock heating of the fuel.[2,5] Any additional irreversible heating sources such as suprathermal or hot electrons ($T_{hot} > 20$ keV) produced by laser–plasma interactions need to be understood and controlled. This article reports, for the first time, evidence of hot-electron production during the early-time burnthrough of the LEH window, which, if not properly controlled, could lead to unacceptably large hot-electron preheat of the DT fuel in an ignition capsule.

The experimental signature of suprathermal-electron generation is the hard x-ray bremsstrahlung emission from small angle scattering of the hot electrons in the high-Z wall of the hohlraum target.[6] The possible sources of hot-electron generation are parametric processes that produce electron-plasma waves, such as two-plasmon-decay ($2\omega_{pe}$) instability[7,8] and stimulated Raman scattering (SRS).[8,9] The $2\omega_{pe}$ instability occurs near quarter-critical density when the phase-matching conditions are satisfied for the laser light to decay into two electron-plasma waves or plasmons. SRS involves the decay of a laser photon into a plasmon and a scattered photon in the visible spectrum. Wave–particle interactions (e.g., Landau damping, trapping, and wave breaking) can generate hot electrons.[8] In addition to hard x rays, an experimental signature of $2\omega_{pe}$ instability is significant $3/2\omega$ emission, which is Thomson scattering of the laser drive from the plasmons.

This article shows, for the first time, that gas-filled hohlraums driven with 13.5 kJ of 351-nm laser light produce two bursts of suprathermal electrons that are clearly resolved with the shaped laser pulse drive having a lower-intensity foot pulse followed by a higher-intensity main drive. The first burst from the two-plasmon-decay ($2\omega_{pe}$) instability in the exploding LEH window produces up to 20 J of hot electrons with $T_{hot} \sim 75$ keV. It has a sharp laser-intensity threshold when the overlapped beam intensity is around 0.5×10^{15} W/cm^2. The $2\omega_{pe}$ instability has been observed in direct-drive ICF;[10] however, this is the first observation of the $2\omega_{pe}$ instability for indirect-drive ICF using 351-nm laser light. The second pulse with $T_{hot} \sim 20$ keV coincides with the SRS during the main laser drive. Previous hard x-ray experiments were not sensitive to the production of window hot electrons because they were time integrated.[6] Window hot electrons were also not observed using an x-ray spectroscopic technique.[11] Only a single burst of hard x rays is observed from a vacuum hohlraum because it does not have a gas fill contained by an LEH window.

Gas-filled Au hohlraums were irradiated on the OMEGA Laser System[12] with 40 beams arranged in three cones and smoothed with phase plates.[13] The thickness of the Au hohlraum wall ranged from 2 to 5 μm, and the hohlraum length varied from 2.3 to 2.55 mm. The inside diameter was 1.6 mm and

the LEH diameter varied from 1.07 to 1.2 mm. Figure 115.32 shows a computer rendering of the hohlraum and the energy-deposition regions of the cone 1, cone 2, and cone 3 beams having angles of incidence to the hohlraum axis of 21.4°, 42.0°, and 58.8°, respectively. Best focus of all the beams occurred at the LEH. Cone 2 and cone 3 beams were pointed to the center of the LEH and contributed to the peak overlapped laser intensity. Cone 1 beams were pointed slightly outside the center of the LEH and did not overlap the other beams at the LEH. All of the hohlraums, except for the vacuum ones, had a 0.6-μm-thick polyimide window, which is close to the 0.5-μm LEH window thickness of the NIF target. As shown in Table 115.I, the initial fully ionized electron density n_e of the hohlraum gas fill was varied by changing the gas fill, where the critical density is given as $n_{cr} = 1.1 \times 10^{21}/\lambda_{\mu m}^2 \text{cm}^{-3} = 9.0 \times 10^{21}\,\text{cm}^{-3}$. The measured laser power of the shaped laser pulse drive (PS26) is shown in Fig. 115.33. The total on-target laser energy E_{UV} was 13.5 kJ. The peak foot power was adjusted to vary the overlapped laser intensity at the LEH window from 0.5 to 1.5 $\times$ 10^{15} W/cm^2. The laser burned through the LEH window with the lower-intensity foot and produced peak radiation temperatures of ~190 eV during the higher-intensity main drive.

The hard x-ray diagnostic (HXRD) has four high-pass energy channels recording time-resolved measurements along a line of sight 42° to the hohlraum axis.[14] The channels have the following lower-energy cutoffs: $h\nu > 20$ keV (HXRD1), $h\nu > 40$ keV (HXRD2), $h\nu > 60$ keV (HXRD3), and $h\nu > 80$ keV (HXRD4). The HXRD has a 120-ps rise time and a 1/e decay time of 1.2 ns. The absolute time scale was established using the hard x rays emitted from a Au spherical target irradiated with an ~200-ps

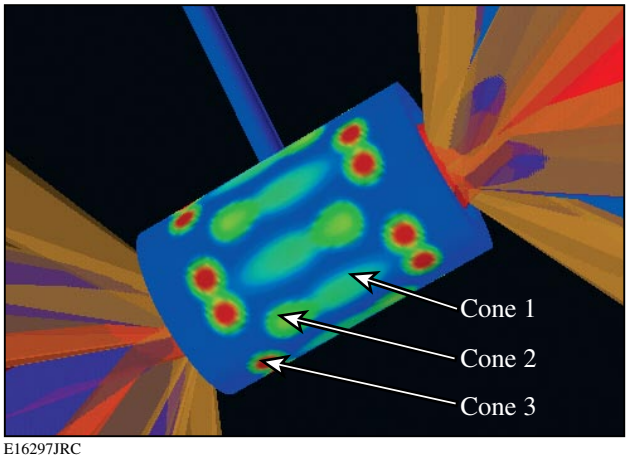

E16297JRC

Figure 115.32
Computer rendering of a gas-filled Au hohlraum irradiated with 40 laser beams. The beams are arranged in three cones and have elliptical phase plates. The energy-deposition regions of cone 1, cone 2, and cone 3 beams are shown on the inner wall of the hohlraum. A shaped laser pulse delivers 13.5 kJ of 351-nm light.

Table 115.I: Hohlraum specifications.

Gas Fill	Pressure (atm)	Initial Fully Ionized n_e
100% CH_4	0.9	0.02 n_{cr}
76% CH_4 + 24% C_5H_{12}	0.9	0.04 n_{cr}
100% C_5H_{12}	0.9	0.1 n_{cr}

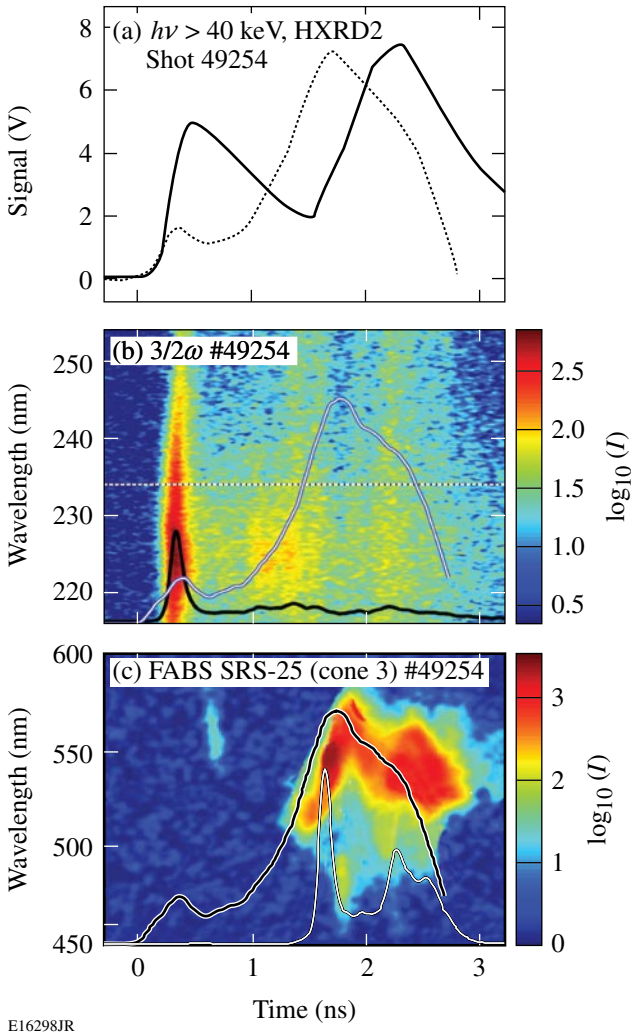

E16298JR

Figure 115.33
(a) Time history of HXRD2 ($h\nu > 40$ keV) (solid curve) compared with laser power (dotted curve). (b) Time-resolved spectral measurement of 3/2ω emission compared with measured laser pulse (white/black curve). Spectrally integrated time history is superposed (white curve). (c) Time-resolved FABS SRS with spectrally integrated time history (white curve) and laser power (white/black curve) superposed.

Gaussian laser pulse. The fraction f_{hot} of laser energy E_{UV} coupled to hot electrons (i.e., $E_{hot} = f_{hot} E_{UV}$) and the temperature characterizing the Maxwellian distribution of hot electrons T_{hot} were inferred from the HXRD measurements using the thick-target bremsstrahlung radiation approximation

$$\frac{dI}{d\nu d\Omega} = \frac{5 \times 10^{11}}{4\pi} E_{hot} \frac{Z}{79} \exp\left(1 - \frac{h\nu}{T_{hot}}\right) \text{keV/keV/sr},$$

where Z is the atomic number of the hohlraum wall material.[6] The attenuation of the lower-energy hard x rays by the Au hohlraum wall was included in the analysis. An *in-situ* calibration was performed on the HXRD using the hard x-ray emission spectrum from a vacuum Au hohlraum irradiated with an 18-kJ, 1-ns square laser pulse. The calibration relied on earlier hohlraum hard x-ray measurements taken on the NOVA laser: the hard x-ray emission from a vacuum Au hohlraum was measured with the filter fluorescer experiment diagnostic,[6] and a Maxwellian distribution of hot electrons with T_{hot} = 30 keV and f_{hot} = 0.3% to 1.0% was inferred from the hard x-ray measurements.[15] The calibration of the HXRD on OMEGA used T_{hot} = 30 keV and f_{hot} = 1%; therefore, the estimates of E_{hot} reported in this article represent upper limits. The uncertainty in the absolute value of E_{hot} does not affect the scaling of hot-electron production with the overlapped laser intensity on the window nor the inferred values of T_{hot}. The $3/2\omega$ emission from the LEH was recorded with a 100-ps temporal resolution and a 0.5-nm spectral resolution.[16] The SRS scattered directly back into the OMEGA lens of a cone 3 beam was recorded with a full-aperture backscatter station (FABS).[16]

The time history of HXRD2 (solid curve) recorded on shot number 49254 for a gas-filled Au hohlraum is compared with the PS26 laser pulse (dotted curve) in Fig. 115.33(a). The peak overlapped foot intensity was $\sim 1.2 \times 10^{15}$ W/cm^2 and the initial fully ionized n_e of the gas fill was 0.1 n_{cr}. The first burst of hard x rays occurs around the time of peak laser foot power, while the second burst of hard x rays occurs around the time of peak laser power. The long decay times of the HXRD measurements are instrumental; nevertheless, the diagnostic has enough temporal resolution to resolve the two bursts of hard x-ray emission. The x-ray fluences of the first and second hard x-ray pulses were calculated for each of the four energy channels, and T_{hot} and f_{hot} were quantified using a least-squares-fitting routine. The time-resolved $3/2\omega$ spectrum is shown in Fig. 115.33(b) and the time-resolved FABS SRS in Fig. 115.33(c). Overplotted on the streaked spectra in Figs. 115.33(b) and 115.33(c) are the laser power and the spectrally integrated scattered-light signals. As can be seen in Fig. 115.33, the first x-ray pulse correlates with the $3/2\omega$ emission during the foot of the laser drive, and the second x-ray pulse correlates with the FABS SRS during the main drive.

The dependence of hot-electron production on the initial hohlraum n_e was investigated, with the peak overlapped foot intensity at the LEH around 1.2×10^{15} W/cm^2. As n_e was increased from 0.02 n_{cr} to 0.1 n_{cr}, f_{hot} for the first hard x-ray pulse increased from 0.005% to 0.1% and T_{hot} increased from 50 to 75 keV. As n_e was increased from 0 to 0.1 n_{cr}, f_{hot} for the second hard x-ray pulse increased from 0.1% to 5% and T_{hot} remained constant around 20 keV. The difference in T_{hot} for the first and second hard x-ray pulses is due to the higher phase velocity of the electron-plasma waves generated by the $2\omega_{pe}$ instability compared to those created by SRS.

The overlapped laser intensity on the LEH was varied from 0.5 to 1.5×10^{15} W/cm^2, and the intensity scaling of hot-electron generation in the exploding LEH window was investigated. The results are shown in Fig. 115.34(a) for E_{hot} with a very sharp threshold just above 0.5×10^{15} W/cm^2. The circles and triangles represent the lower ($n_e = 0.04\ n_{cr}$) and higher ($n_e = 0.1\ n_{cr}$) electron densities, respectively. The total energy in hot electrons, E_{hot}, is approximately 20 J with the higher n_e and an overlapped LEH laser intensity of $\sim 1.2 \times 10^{15}$ W/cm^2. The production of window hot electrons for the NIF-like density ($n_e = 0.04\ n_{cr}$) with the high overlapped intensity is between 2 and 5 J. The scaling of T_{hot} with the overlapped LEH intensity is shown in Fig. 115.34(b). The hohlraums with $n_e = 0.1\ n_{cr}$ and the highest overlapped intensity have $T_{hot} \sim 75$ keV. More scatter in T_{hot} (40 keV < T_{hot} < 80 keV) is observed for the hohlraums with $n_e = 0.04\ n_{cr}$ and the highest overlapped intensity. The measurements with the lowest overlapped intensity show a decrease in T_{hot} to ~30 keV. The OMEGA experiment is an excellent surrogate for the production of window hot electrons on the NIF ignition hohlraum: 2-D simulations from the radiation hydrodynamics code *HYDRA*[17] show that the window burnthrough phase of the gas-filled OMEGA hohlraum is hydrodynamically similar to that of an ignition hohlraum.

The linear theory of Simon *et al.* for the $2\omega_{pe}$ instability[7] predicts the threshold and growth rate of the instability, as well as the hot-electron temperature T_{hot} of electrons trapped in the plasmons; however, it does not predict the total energy in the trapped electrons. This requires determining the amplitude of the plasma waves, the trapping rate of electrons in the waves, and the competition between trapping and other wave saturation mechanisms, such as collisions. For the simulated

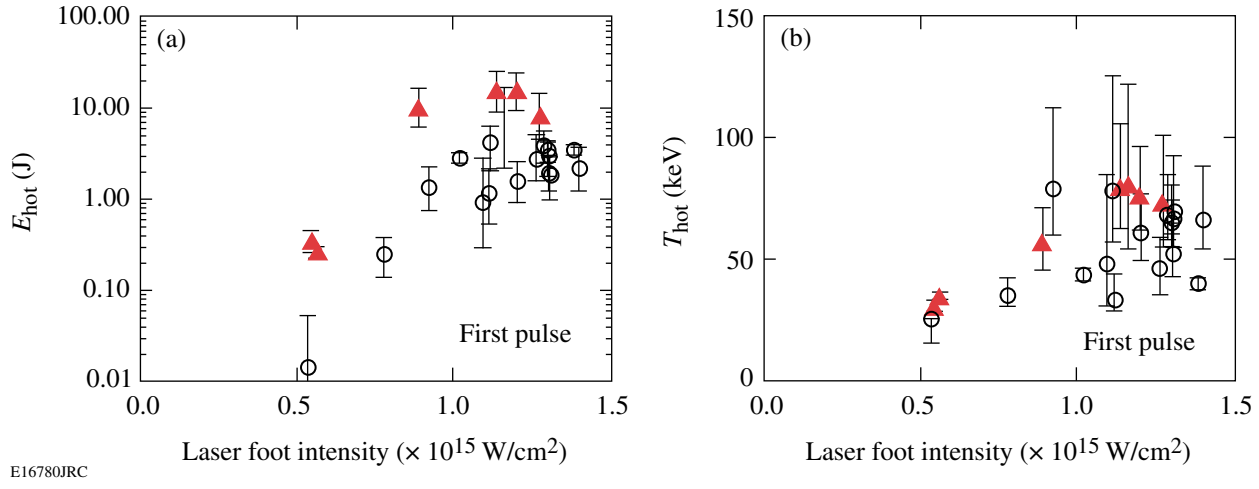

Figure 115.34
Scaling of (a) E_{hot} and (b) T_{hot} with the peak overlapped laser intensity on the LEH window for $n_e = 0.04\ n_{cr}$ (circles) and $n_e = 0.1\ n_{cr}$ (triangles).

electron temperatures in the exploding window of an OMEGA hohlraum, the linear theory of the $2\omega_{pe}$ instability predicts $T_{hot} \geq 70$ keV, which is consistent with measurements during the early part of the laser pulse.

The $2\omega_{pe}$ instability occurs only in the vicinity of plasma at $n_e = 0.25\ n_{cr}$. The threshold intensity for the $2\omega_{pe}$ instability, $I_{thresh} \propto T_e/\lambda L$, is a function of the laser wavelength λ, electron temperature T_e, and density gradient scale length in the direction of the laser beam, $L = n_e\left(\partial n_e/\partial x\right)^{-1} = \left(n_{cr}/4\right)\left(\partial n_e/\partial x\right)^{-1}$. Motivated by recent direct-drive experiments,[10] the overlapped beam intensity is used in the threshold formula rather than the intensity of a single beam. This lower threshold is likely due to cooperative excitation of a common forward-directed plasma wave and/or to effects, such as swelling in intensity and increased interaction length for incident light waves that turn near the quarter-critical density.

Using 2-D radiation hydrodynamic simulations from the code *HYDRA*, it is possible to determine the laser power P_{pass} that passes the $n_e = 0.25\ n_{cr}$ surface with intensity above the threshold. The energy at risk of scattering into two plasmons is then given by

$$E_{risk} = \int_t \max\left(0, P_{pass} - P_{thresh}\right) dt$$
$$= \int_t dt \sum_N P_{ray} \max\left(0, \frac{I_{pass} - I_{thresh}}{I_{thresh}}\right).$$

Here, P_{pass}–P_{thresh} is the laser power with intensity $I > I_{thresh}$ and P_{ray} is the power of each of the N computed laser rays as it crosses the $n_e = 0.25\ n_{cr}$ surface. In *HYDRA*, the average intensity, defined as the amount of power traversing a zone, is used to represent the overlap intensity I. This expression does not predict E_{hot} since it does not include the efficiency at which the $2\omega_{pe}$ instability generates hot electrons; however, the threshold given above can qualitatively explain the observed scalings of E_{hot} with hohlraum gas-fill density and laser intensity.

The two factors that determine the energy at risk for the $2\omega_{pe}$ instability are the fraction of the laser flux that crosses a surface of density $n_e = 0.25\ n_{cr}$ and the intensity of the laser at that surface. When the laser beams initially ablate the 0.6-μm-thick polyimide LEH window, they launch a shock wave. As the window plasma expands to low density, the laser-energy–deposition rate drops. The shock wave becomes unsupported and transits into the gas plasma behind the window as a hemispherical blast wave. When the blast wave expands below $n_e = 0.25\ n_{cr}$ everywhere, the risk of the $2\omega_{pe}$ instability in the LEH region is gone.

For hohlraums with an initial gas plasma density of $n_e = 0.04\ n_{cr}$, *HYDRA* simulations show that the blast-wave density is below $n_e = 0.25\ n_{cr}$ as soon as it enters the gas region. For the $n_e = 0.10\ n_{cr}$ hohlraums, the blast-wave peak density remains above $n_e = 0.25\ n_{cr}$ for about 0.1 ns after the blast wave enters the gas plasma. *HYDRA* simulations predict that E_{risk} should drop by a third between $n_e = 0.10\ n_{cr}$ and $n_e = 0.04\ n_{cr}$, which is consistent with the upper range of the points in Fig. 115.34(a). Post-processed *HYDRA* simulations confirm that E_{risk} decreases with intensity; however, this predicted scaling is too slow to explain the rapid drop in E_{hot} observed for intensities below 10^{15} W/cm^2. Presumably, the observed

drop is due to a decrease in the efficiency of trapping and accelerating electrons in the plasmons, which is not modeled in the expression for E_{risk}.

The observed threshold for the window hot electrons can be exploited to mitigate the hot-electron production as the LEH window burns through in gas-filled hohlraums. Specifications for the NIF ignition target restrict E_{hot} to less than 8 J for T_{hot} = 70 keV and to less than 38 J for T_{hot} = 30 keV; otherwise, preheat of the implosion capsule could jeopardize hot-spot ignition. As a result of this research, the initial overlapped laser intensity incident on the LEH window of an ignition target for the NIF has been set below the measured intensity threshold to retain ignition margin by staggering the turn-on time of the inner and outer cones of beams.

Two bursts of suprathermal electrons are observed from gas-filled hohlraums driven with 351-nm laser light. The $2\omega_{\text{pe}}$ instability in the exploding LEH window appears to produce up to 20 J of hot electrons with $T_{\text{hot}} \sim 75$ keV at early times and has a sharp laser-intensity threshold around 0.5×10^{15} W/cm^2. The observed threshold can be exploited to mitigate the hot-electron production in hohlraums. Simulations using a 2-D radiation hydrodynamics code and a linear theory of the $2\omega_{\text{pe}}$ instability show qualitative agreement with the experimental results. The second pulse produced by SRS during the main laser drive has more energy, but significantly lower $T_{\text{hot}} \sim 20$ keV.

ACKNOWLEDGMENT

The authors acknowledge the superb operation of the OMEGA Laser System, the target fabrication expertise of M. Bonino at LLE and A. Nikroo at General Atomics, and the diagnostic expertise of R. Bahr and S. Roberts at LLE. This work was supported by the U.S. Department of Energy Office of Inertial Confinement Fusion under Cooperative Agreement No. DE-FC52-08NA28302, the University of Rochester, and the New York State Energy Research and Development Authority. The support of DOE does not constitute and endorsement by DOE of the views expressed in this article.

REFERENCES

1. R. L. McCrory, D. D. Meyerhofer, R. Betti, R. S. Craxton, J. A. Delettrez, D. H. Edgell, V. Yu Glebov, V. N. Goncharov, D. R. Harding, D. W. Jacobs-Perkins, J. P. Knauer, F. J. Marshall, P. W. McKenty, P. B. Radha, S. P. Regan, T. C. Sangster, W. Seka, R. W. Short, S. Skupsky, V. A. Smalyuk, J. M. Soures, C. Stoeckl, B. Yaakobi, D. Shvarts, J. A. Frenje, C. K. Li, R. D. Petrasso, and F. H. Séguin, Phys. Plasmas **15**, 055503 (2008).

2. J. D. Lindl *et al*., Phys. Plasmas **11**, 339 (2004).

3. J. A. Paisner, E. M. Campbell, and W. J. Hogan, Fusion Technol. **26**, 755 (1994); G. H. Miller, E. I. Moses, and C. R. Wuest, Opt. Eng. **43**, 2841 (2004).

4. J. Schein *et al*., Phys. Rev. Lett. **98**, 175003 (2007); O. S. Jones *et al*., Phys. Plasmas **14**, 056311 (2007).

5. M. C. Herrmann, M. Tabak, and J. D. Lindl, Nucl. Fusion **41**, 99 (2001); R. Betti, K. Anderson, V. N. Goncharov, R. L. McCrory, D. D. Meyerhofer, S. Skupsky, and R. P. J. Town, Phys. Plasmas **9**, 2277 (2002).

6. R. P. Drake *et al*., Phys. Rev. A **40**, 3219 (1989); J. W. McDonald *et al*., Rev. Sci. Instrum. **75**, 3753 (2004); J. W. McDonald *et al*., Phys. Plasmas **13**, 032703 (2006).

7. D. W. Phillion *et al*., Phys. Rev. Lett. **49**, 1405 (1982); D. M. Villeneuve, R. L. Keck, B. B. Afeyan, W. Seka, and E. A. Williams, Phys. Fluids **27**, 721 (1984); C. Rousseaux *et al*., Phys. Fluids B **4**, 2589 (1992); W. Seka, R. E. Bahr, R. W. Short, A. Simon, R. S. Craxton, D. S. Montgomery, and A. E. Rubenchik, Phys. Fluids B **4**, 2232 (1992); C. S. Liu and M. N. Rosenbluth, Phys. Fluids **19**, 967 (1976); A. Simon, R. W. Short, E. A. Williams, and T. Dewandre, Phys. Fluids **26**, 3107 (1983); A. B. Langdon, B. F. Lasinski, and W. L. Kruer, Phys. Rev. Lett. **43**, 133 (1979); B. F. Lasinski and A. B. Langdon, Lawrence Livermore National Laboratory, Livermore, CA, Report UCRL-50021-77, 4-49 (1978); B. B. Afeyan and E. A. Williams, Phys. Plasmas **4**, 3827 (1997); B. B. Afeyan and E. A. Williams, Phys. Plasmas **4**, 3845 (1997).

8. W. L. Kruer, *The Physics of Laser–Plasma Interactions,* Frontiers in Physics, Vol. 73, edited by D. Pines (Addison-Wesley, Redwood City, CA, 1988), Chap. 4, pp. 37–43.

9. J. W. Shearer *et al*., Phys. Rev. A **6**, 764 (1972); K. Estabrook, W. L. Kruer, and B. F. Lasinski, Phys. Rev. Lett. **45**, 1399 (1980); K. Estabrook and W. L. Kruer, Phys. Fluids **26**, 1892 (1983); A. A. Offenberger *et al*., Phys. Rev. Lett. **49**, 371 (1982); T. P. Hughes, *Plasmas and Laser Light* (Wiley, New York, 1975); B. J. MacGowan *et al*., Phys. Plasmas **3**, 2029 (1996).

10. C. Stoeckl, R. E. Bahr, B. Yaakobi, W. Seka, S. P. Regan, R. S. Craxton, J. A. Delettrez, R. W. Short, J. Myatt, A. V. Maximov, and H. Baldis, Phys. Rev. Lett. **90**, 235002 (2003).

11. S. H. Glenzer *et al*., Phys. Rev. Lett. **81**, 365 (1998).

12. T. R. Boehly, D. L. Brown, R. S. Craxton, R. L. Keck, J. P. Knauer, J. H. Kelly, T. J. Kessler, S. A. Kumpan, S. J. Loucks, S. A. Letzring, F. J. Marshall, R. L. McCrory, S. F. B. Morse, W. Seka, J. M. Soures, and C. P. Verdon, Opt. Commun. **133**, 495 (1997).

13. *LLE Review Quarterly Report* **112**, 212, Laboratory for Laser Energetics, University of Rochester, Rochester, NY, LLE Document No. DOE/SF/19460-790 (2007).

14. C. Stoeckl, V. Yu. Glebov, D. D. Meyerhofer, W. Seka, B. Yaakobi, R. P. J. Town, and J. D. Zuegel, Rev. Sci. Instrum. **72**, 1197 (2001).

15. R. L. Kauffman, Lawrence Livermore National Laboratory, private communication (2008).

16. W. Seka, D. H. Edgell, J. P. Knauer, J. F. Myatt, A. V. Maximov, R. W. Short, T. C. Sangster, C. Stoeckl, R. E. Bahr, R. S. Craxton, J. A. Delettrez, V. N. Goncharov, I. V. Igumenshchev, and D. Shvarts, Phys. Plasmas **15**, 056312 (2008).

17. M. M. Marinak *et al*., Phys. Plasmas **8**, 2275 (2001).